Role of antisite disorder on intrinsic Gilbert damping in $L1_0$ FePt films

X. Ma,[1] L. Ma,[2] P. He,[2] H. B. Zhao,[3,*] S. M. Zhou,[2] and G. Lüpke[1,†]

[1]*Department of Applied Science, College of William and Mary, 251 Jamestown Road, Williamsburg, Virginia 23187, USA*

[2]*Shanghai Key Laboratory of Special Artificial Microstructure Materials and Technology and School of Physics Science and Engineering, Tongji University, Shanghai 200092, China*

[3]*Key Laboratory of Micro and Nano Photonic Structures (Ministry of Education), Department of Optical Science and Engineering, Fudan University, Shanghai 200433, China*

The impact of antisite disorder x on the intrinsic Gilbert damping α_0 in well-ordered $L1_0$ FePt films is investigated by time-resolved magneto-optical Kerr effect. The variation of x mainly affects the electron scattering rate $1/\tau_e$, while other leading parameters remain unchanged. The experimentally observed linear dependence of α_0 on $1/\tau_e$ indicates that spin relaxation is through electron interband transitions, as predicted by the spin-orbit coupling torque correlation model. Measurements at low temperature show that α_0 remains unchanged with temperature even for FePt with very high chemical order, indicating that electron-phonon scattering is negligible. Moreover, as x decreases, the perpendicular magnetic anisotropy increases, and the Landau g factor exhibits a negative shift due to an increase in orbital momentum anisotropy. Our results will facilitate the design and exploration of magnetic alloys with large magnetic anisotropy and desirable damping properties.

I. INTRODUCTION

Ultrafast magnetization precessional switching in ferromagnets utilizing magnetic field pulses, spin polarized currents, and ultrafast laser pulses [1–6] is currently a popular topic due to its importance in magnetic information storage and spintronic applications. The uniform magnetization precession can be well modeled with the Landau-Lifshitz-Gilbert-Slonczewski (LLGS) equation [7–9], where the Slonczewski torque term denotes the spin transfer torques (STTs), and the Gilbert damping parameter α determines the spin relaxation time [10] and is crucial for device performance [11–14]. The extrinsic Gilbert damping is due to nonlocal spin relaxation, such as spin pumping and magnon-magnon scattering, which can be tuned by artificial substrates, specially designed buffer and coverage layers [15–21], while the intrinsic Gilbert damping parameter α_0 is thought to arise from spin-orbit interaction (SOI) [22–30], and recently its quadratic dependence on SOI is demonstrated experimentally in FePtPd alloys [31].

The α_0 describes the energy flow rate from spin to electronic orbital and phonon degrees of freedom through electron scattering and has been studied in various theoretical models [22–30]. The breathing Fermi surface model [22] and torque-correlation model [23] based on first-principle band structure calculations qualitatively match α_0 in soft magnetic alloys such as Fe, Co, and Ni [32–37]. Moreover, contributions to α_0 can be categorized based on intraband and interband transitions [23,26]. The damping rate from intraband transitions scales linearly with the electron relaxation time τ_e and exhibits conductivitylike behavior. In contrast, the damping rate from the interband transition is proportional to the electron scattering rate $1/\tau_e$ and consequently exhibits resistivitylike behavior. Therefore, the transition from conductivitylike to resistivitylike behavior through modulation of $1/\tau_e$ is used to

qualitatively understand the temperature dependence of α in soft magnetic materials [23,26].

The underlying physics of α_0 in metallic magnets with large uniaxial magnetic anisotropy K_u, however, is not completely understood. The question is still open as to whether the well-developed theories can shed light on the damping behavior in such materials and therefore motivates extensive research [31,38–43]. For instance, S. Mizukami *et al.* demonstrated a low value of α_0 with considerable K_u in MnGa alloys due to the low density of states at the Fermi level, $D(E_F)$ [40]. One key investigation still missing is the relationship between α_0 and $1/\tau_e$. Theoretical studies [28–30] point out that $1/\tau_e$ involves various types of electron scattering events such as by phonon and impurity. It is difficult to measure the electron-phonon scattering rate from experiments with sufficient accuracy, while the electron-impurity scattering can be controlled by either doping or artificial disorder. However, no direct experiments have been reported to verify quantitatively the relationship between α_0 and $1/\tau_e$ through impurity scattering despite many attempts [33,44–47]. The challenge lies in the fact that α_0 also depends on other leading parameters, such as magnetization M_S [33], SOI [44], lattice distortion [47], and $D(E_F)$ [40], which may vary significantly when the impurity concentration is modulated. It is difficult to quantitatively investigate the impact of $1/\tau_e$ on α_0 in those material systems.

In this paper, we investigate the effect of antisite disorder on α_0 in well-ordered $L1_0$ FePt thin film samples. Time-resolved magneto-optical Kerr effect (TRMOKE) measurements show that α_0 gradually increases by more than a factor of three when the antisite disorder x is varied from 3 to 16% by sample growth temperature (T_g). The variation of x mainly affects the electron scattering rate $1/\tau_e$, while other leading parameters remain almost unchanged. A linear correlation between α_0 and $1/\tau_e$ is experimentally observed due to electron interband transitions. Moreover, α_0 remains unchanged down to low temperature (20 K), indicating that the electron-phonon interaction and electron intraband transitions are negligible. In addition, K_u

*hbzhao@fudan.edu.cn

†gxluep@wm.edu

decreases, and the Landau g factor increases with larger x due to an increase in orbital momentum anisotropy. Our results provide a pathway for designing magnetic alloys with desirable α and K_u.

II. EXPERIMENTS

A series of $L1_0$ ordered FePt thin films are deposited on single crystal MgO (001) substrates by magnetron sputtering. The FePt composite target is fabricated by placing small Pt pieces on a Fe target. The base pressure of the deposition system is $1.0 * 10^{-5}$ Pa, and the Ar pressure is 0.35 Pa. During deposition, the rate of deposition was about 0.1 nm/s, and the substrates are kept at different temperatures T_g. After deposition, the samples are annealed *in situ* at the same temperature as their growth temperature for 2 hours. Two series of samples with different thickness are fabricated, and the film thickness is determined by x-ray reflectivity to be 17 ± 1 nm and 22 ± 1 nm. The microstructure analysis is performed by using x-ray diffraction (XRD), with Cu $K\alpha$ radiation. Static magnetization hysteresis loops are measured by vibrating sample magnetometer (VSM) at room temperature.

In order to measure α, TRMOKE measurements are performed at various temperatures T with a pump-probe setup using pulsed Ti:sapphire laser with a pulse duration of 200 fs and a repetition rate of 250 kHz. The wavelength of pump (probe) pulses is 400 nm (800 nm). A modulated pump pulse beam with a fluence of $0.16\,\mathrm{mJ/cm^2}$ is focused to a spot $\sim$1 mm in diameter on the sample to excite the magnetization precession, and the transient Kerr signal is detected by a probe pulse beam that is time-delayed with respect to the pump. The focus area of the probe beam has a diameter of 0.7 mm, which was smaller than that of the pump beam so that the intensity ratio of the pump to probe pulses is set to be about 6:1. The geometry of applied external magnetic field and magnetization precession is depicted in Fig. 1(a). A variable magnetic field H up to 6.5 T is applied at an angle of $\theta_H = 45°$ with respect to the film normal direction using a superconducting magnet [48].

III. RESULTS AND DISCUSSION

A. Sample characterization

Figure 1(b) displays the out-of-plane magnetization hysteresis loops for 22-nm-thick films with $T_g = 580°$C, $620°$C, and $680°$C and the in-plane hysteresis loop for the sample with $T_g = 620°$C. The out-of-plane hysteresis loops are almost square-shaped with coercivity $H_c = 0.3$ T, but it is difficult to reach the saturated magnetization with in-plane magnetic field, indicating the establishment of high perpendicular magnetic anisotropy K_u. From the experiments, the saturation magnetization M_S for all samples is determined to be 1100 emu/cm³ and remains unchanged as a function of growth temperature and disorder x. Moreover, the magnetization is not fully saturated with $H = 2$ T applied along the easy axis, indicating the existence of multiple magnetic domains at lower magnetic fields.

Figure 1(c) displays the structure characterization of FePt samples with XRD measurements. Only face-centered-tetragonal (fct) (001) and (002) peaks of FePt are observed in the spectrum along with other peaks from MgO substrate,
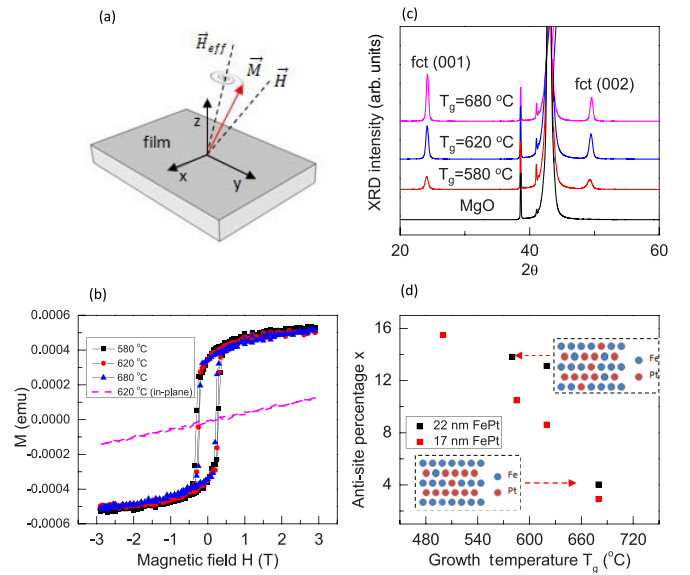

FIG. 1. (Color online) Schematic of TRMOKE measurement geometry (a), static magnetic hysteresis loops measured by VSM (b), structure characterization results of FePt thin films by XRD (c), and antisite disorder percentage x as a function of growth temperature T_g (d). The insets in (d) depict FePt alloy structure with low (left) and high (right) antisite disorder concentration.

which indicates the $L1_0$ ordering in the FePt alloys. The peak positions do not shift with different T_g, which indicates that the lattice constant varies by less than 1.0% for different T_g, and tetragonal distortion of lattice is not affected. The antisite disorder percentage is derived from

$$x = \frac{1-S}{2} = \left(1 - \sqrt{\frac{\left(\frac{I_{001}}{I_{002}}\right)_{\mathrm{meas}}}{\left(\frac{I_{001}}{I_{002}}\right)_{\mathrm{calc}}}}\right)/2, \qquad (1)$$

where S is the degree of chemical order, I_{001} and I_{002} are integrated intensities of fct (001) and (002) peaks, and $(1-x)$ is the probability of the correct site occupation for either Fe or Pt atoms in such an $L1_0$ ordered alloy system [49]. $(I_{001}/I_{002})_{\mathrm{calc}}$ is calculated to be 2.0 for the perfect ordered film with thickness ranging from 11 to 49 nm [49]. The x as a function of T_g for films with both thicknesses is shown in Fig. 1(d). Higher T_g leads to monotonous decrease of the antisite disorder x in FePt alloys, as depicted by the insets in Fig. 1(d).

Islands form throughout the film with $T_g = 720°$C or $740°$C, which prevents further sole reduction of bulk point defects. Figure 2 displays the surface topography from samples prepared at $T_g = 620°$C and $T_g = 720°$C with scanning electron microscopy (SEM). With $T_g \leqslant 680°$C, the FePt layer is homogeneously distributed throughout the thin film, as indicated in Fig. 2(a). In contrast with $T_g = 720°$C or $740°$C, the FePt layer is inhomogeneously distributed on the MgO substrate, and islands form. As shown in Fig. 2(b), the dark contrast in the image corresponds to areas without FePt grown on the MgO substrate. The formation of islands and particles in $L1_0$ ordered FePt thin films leads to lower chemical order as the Fe-rich clusters are promoted at the surface regions [50]. Moreover, it will also introduce more surface contribution to
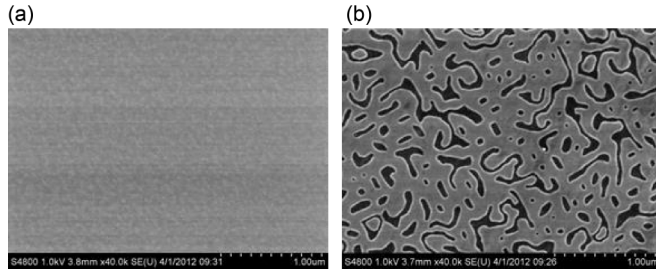
FIG. 2. SEM results from FePt thin films grown at $T_g = 620\,^\circ$C (a) and $T_g = 720\,^\circ$C (b).

the magnetic properties, such as K_u, g factor, and damping. For instance, the islands exhibit pronounced out-of-plane anisotropy K_u, which is peaked when $c = 0.5$ in $Fe_cPt_{(1-c)}$ alloys [50]. This is due to Dzyaloshinskii-Moriya interactions emerging at the surface as a result of the broken inversion symmetry, which compete with exchange interactions causing the complex magnetism at the FePt surface. With respect to the impact on the g factor, the orbital momentum is not entirely quenched due to the broken symmetry at the surface, while the formation of islands or enlarged surface areas results in a negative shift of g factor [51].

B. Gilbert damping

Figure 3(a) shows the TRMOKE results of FePt thin films with various x at $H = 6.5$ T. The uniform magnetization precession is demonstrated by the oscillatory Kerr signals θ_K, while the magnetic damping is indicated by the decaying precession amplitude as the time delay increases. The measured

θ_K can be well fitted by the following equation:

$$\theta_K = a + b^* \exp(-t/t_0) + A^* \exp(-t/\tau) \sin(2\pi f t + \varphi),$$

(2)

where parameters A, τ, f, and φ are the amplitude, magnetic relaxation time, spin precession frequency, and initial phase of the magnetization precession, respectively [31]. Here, a, b, and t_0 correspond to the background signal owing to the slow recovery process after fast demagnetization by laser pulse heating. It is well demonstrated in Fig. 3(a) that the spin precession frequency is larger and the magnetic damping effect becomes weaker for lower x with the same H.

In order to obtain α for FePt samples with different x, magnetic field (H)-dependent TRMOKE measurements are performed. Figure 3(b) shows the measured results of the 22-nm-thick sample with $T_g = 680\,^\circ$C. It can be seen clearly that the precession period and relaxation time vary as H increases. The fitted f as a function of H for different x are plotted in Fig. 3(c). We note that f can be tuned from 225 to 335 GHz by varying H and x. By solving the LLG equation, f can be expressed as

$$2\pi f = \gamma (H_1 H_2)^{1/2},$$

(3)

where $H_1 = H \cos(\theta_H - \theta) + H_K \cos^2\theta$, $H_2 = H \cos(\theta_H - \theta) + H_K \cos 2\theta$, $H_K = 2K_u/M_S - 4\pi M_S$, and $\gamma = \gamma_e g/2$, with $\gamma_e = 1.76 \times 10^7$ Hz/Oe, Landau g factor, saturated magnetization $M_S = 1100$ emu/cm^3, and perpendicular anisotropy K_u. The equilibrium angular position θ of the magnetization satisfies the equation $\sin 2\theta = (2H/H_K) \sin(\theta_H - \theta)$. The measured H dependence of f can be well fitted by Eq. (3), as shown in Fig. 3(c), and we thus obtain K_u and g. K_u decreases from 5.2 to 3.2 (10^7 erg/cm^3), and the Landau g factor also displays a shift from 1.9 to 2.24 as x increases, as shown in Fig. 4(a). Furthermore, using the fitted values of τ,
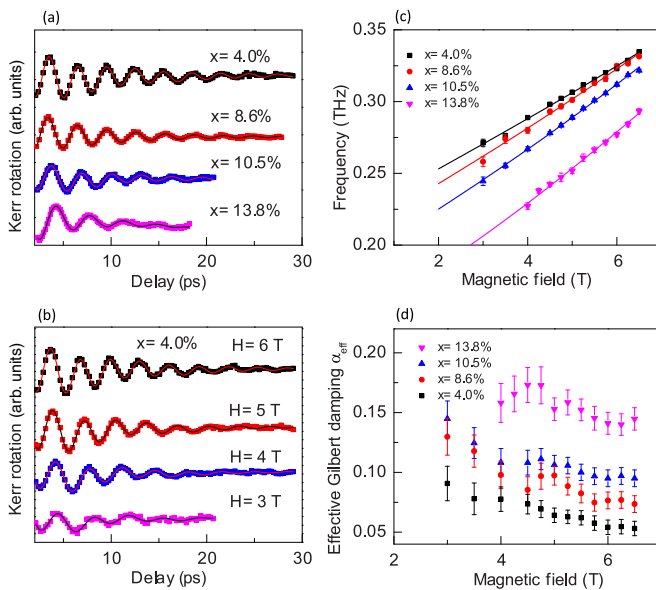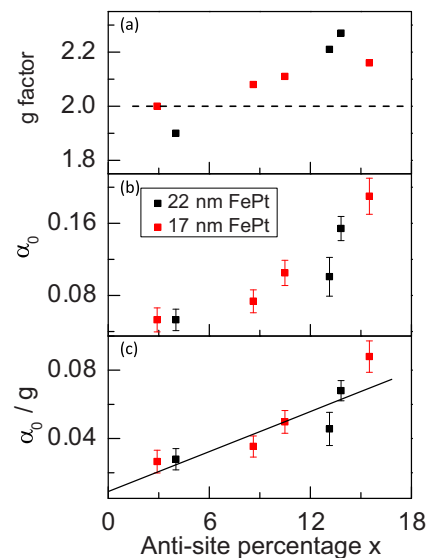

FIG. 3. (Color online) TRMOKE data from FePt thin films with different x and applied magnetic field $H = 6.5$ T (a) and with $x = 4\%$ measured at different H (b). The dependence of spin precession frequency f (c) and effective Gilbert damping α_{eff} (d) on H obtained from Eqs. (2) and (4) for FePt thin films with different x. The solid lines refer to fitted results using Eqs. (2) and (3).

FIG. 4. (Color online) Landau g factor (a), intrinsic Gilbert damping α_0 (b), and α_0/g (c) as a function of antisite defect concentration x for FePt films with thicknesses of 17 nm and 22 nm.

we determine the effective Gilbert damping α_{eff} with

$$\alpha_{\text{eff}} = \alpha_0 + \alpha_{\text{ex}} = \frac{2}{\tau \gamma (H_1 + H_2)}, \qquad (4)$$

where α_{ex} is the extrinsic contribution to Gilbert damping [40]. As shown in Fig. 3(d), the value of α_{eff} gradually decreases with higher H and saturates at high fields [52]. The decreasing trend of α_{eff} with H is attributed to the suppression of dephasing dynamics among magnetic domains [21,31] since multiple domains exist at low fields, as indicated in Fig. 1(b), and the magnon-magnon scattering is less effective for perpendicularly magnetized samples [53]. The saturation values of α_{eff} at higher fields are therefore used to approximate the intrinsic Gilbert damping α_0 [31]. Figure 4(b) shows α_0 as a function of x at $T = 200$ K.

The key finding here is that α_0 gradually increases with larger x. Since the scattering rate $1/\tau_e$ is enhanced with more impurity scattering sites x according to scattering theory [28–30], the positive correlation between α_0 and $1/\tau_e$ qualitatively matches the resistivitylike behavior where α_0 is governed by interband transitions [23,26]. In the spin-orbit coupling torque correlation model for interband transitions [23,26,40],

$$\alpha_0 \propto \frac{g\mu_B{}^2 D(E_F)\xi^2}{M_S W^2 \tau_e}, \qquad (5)$$

where W is the d band width, ξ the spin-orbit coupling strength, and $D(E_F)$ is the density of states at Fermi level. It is demonstrated that antisite disorder in $L1_0$ ordered alloys smoothens the density of states [54]. The calculated $D(E_F)$ increases within 5% as x increases, and W remains almost the same [55] when $0 < x < 15\%$, as in our case. In our previous paper [56], we investigated the anomalous Hall conductivity of $L1_0$ ordered FePt films with different ordering. The resistivity-independent term (b_0) of anomalous Hall conductivity remains almost unchanged with x when x is small, indicating that the variance of spin-orbit coupling strength ξ is negligible in our samples. The g factor increases by 19% with larger x, as shown in Fig. 4(a), due to the modulation of orbital momentum anisotropy (discussed in the next subsection). The lattice distortion and M_S remain almost unchanged, as demonstrated by structure characterization and VSM measurements. A similar trend of α_0 with x is observed for samples with two different thicknesses, which indicates that surface and strain effects on damping can be ruled out. Therefore, we attribute the significant increase of α_0 by more than three times, as revealed in Fig. 4(b), to the enhancement of $1/\tau_e$ as a result of the increasing x. To separate the effect of g on the damping, we further plot α_0/g as a function of x in Fig. 4(c). We observe approximately a linear correlation between the two variables. The exchange of different types of atoms in $L1_0$ ordered alloy film leads to the scattering of itinerant electrons through local spin-dependent exchange potentials. Since the cross-section and strength of individual scattering events remain unchanged in weak scattering regime [28], the linear correlation indicates that α_0 is proportional to $1/\tau_e$, where the damping process is dominated by interband contribution [57]. The damping process can be considered roughly as the decay of a uniform mode magnon into an electron spin-flip excitation. Therefore, the antisite disorder works as spin-flip scattering center for itinerant electrons transferring spin angular momentum to the
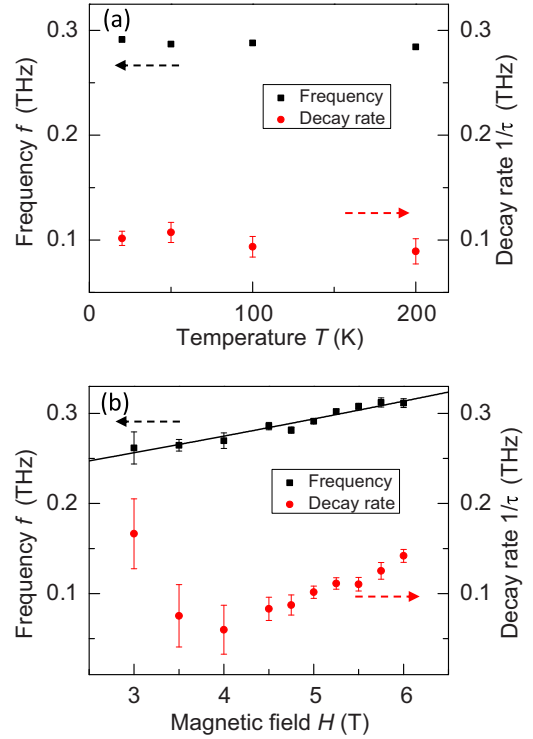

FIG. 5. (Color online) The f and $1/\tau$ as functions of temperature T with applied field $H = 5$ T (a) and as functions of H at 20 K (b). The solid lines refer to fitted results using Eq. (3).

lattice via SOI. Moreover, complete suppression of the antisite defects might lead to a remnant α_0, where the electron is mainly scattered by phonon instead of impurity.

In order to check for intraband contribution to α_0, temperature-dependent TRMOKE measurements are carried out. The TRMOKE measurements are carried out for the 17-nm-thick FePt film with the lowest $x = 3\%$ at low temperatures. Figure 5(a) shows that the frequency and decay rate of coherent spin precession at $H = 5$ T varies slightly with temperature (from 20 to 200 K). The field-dependent frequency and decay rate at 20 K, as shown in Fig. 5(b), are analyzed to obtain α_0. It turns out that α_0 remains almost unchanged (from 0.053 ± 0.013 to 0.054 ± 0.013) when temperature decreases from 200 to 20 K, despite a significant change in the electron-phonon scattering rate [23,26]. The temperature-independent behavior of α_0 indicates that electron-phonon scattering is negligible, and electron-impurity interaction dominates the scattering events. In our previous paper [31], we calculated the electron-phonon scattering rate from first principles to be approximately 1.33 ps^{-1} for FePt at 200 K. The electron-impurity scattering rate must be considerably higher. Moreover, the weak temperature dependence of α_0 indicates that the 3% antisite disorder is still too high to observe the conductivitylike behavior for intraband contribution to α_0, which may become significant with low $1/\tau_e$. Further investigations at low temperature with fewer impurities are necessary to get deeper insight on the relationship between α_0 and τ_e governed by intraband transitions.
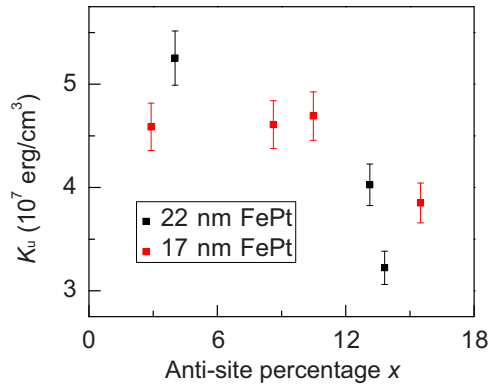
FIG. 6. (Color online) Perpendicular magnetic anisotropy K_u as a function of antisite disorder percentage x.

C. Perpendicular magnetic anisotropy (K_u) and Landau g factor

Figure 6 shows that the K_u maintains high values from 3.2 to 5.2 $(10^7 \, \text{erg/cm}^3)$ and gradually increases with smaller x, which is consistent with other experiments as well as the theory [49,58–61]. The K_u in FePt alloys results from the simultaneous occurrence of the spin polarization and large SOI [62]. The smaller x represents that more Pt atoms become the nearest neighbors of Fe, which results in stronger hybridization between Fe and Pt atoms. Consequently, Pt acquires larger spin polarization and orbital moment due to the Fe-Pt hybridization in the higher chemical ordered sample and contributes significantly to K_u. As a result, the orbital momentum anisotropy is increased [60,61], and K_u is suggested to increase with decreasing x.

Figure 4(a) shows that a gradual decrease of the Landau g factor is observed with smaller x. The g factor sets the proportionality of angular momentum and magnetic moment for the individual spins, which also affects the dynamic response of a magnetic film. In itinerant electron systems, the g factor may be written as

$$g = \frac{2m_e}{e} * \frac{\mu_S + \mu_L}{\langle S' \rangle + \langle L \rangle}, \qquad (6)$$

where μ_S (u_L) denotes the magnetic momentum from the spin (orbital) component, and $\langle S' \rangle$ ($\langle L \rangle$) is the spin (orbital) contribution to the electron angular momentum. For a symmetric crystal lattice, the orbital motion of the d electron is quenched by the crystal field effect, i.e., $\langle L \rangle = 0$. Nevertheless, the orbital contribution to the magnetic moment is nonzero, thus the g factor is equal to $2^*(1 + u_L/\mu_S)$ and is typically greater than two in an itinerant electron system. However, as x decreases, the enhanced hybridization between Fe and Pt restores the orbital momentum due to the large SOI strength of Pt [62] and raises the orbital momentum anisotropy [60,61]. This would lead to $\langle L \rangle \neq 0$ and $g \approx 2^*(1 - u_L/\mu_S)$, indicating a negative shift of the g factor relative to the value of two. Such a negative shift of the g factor is also observed at surface or interface, where the orbital momentum is not entirely quenched due to the symmetry broken effect [51].

IV. CONCLUSION

In conclusion, we demonstrate that in $L1_0$ ordered FePt films, control of the antisite disorder x with proper growth temperature results in significant variation of α_0. As x increases from 3 to 16%, α_0 increases by more than a factor of three from 0.05 to 0.19. The variation of x mainly affects the scattering rate $1/\tau_e$, while other leading parameters remain unchanged. A linear correlation between α_0 and $1/\tau_e$ is observed experimentally due to electron interband transitions. Moreover, α_0 remains unchanged with temperature, indicating that electron-phonon scattering and electron intraband transitions are negligible. Moreover, as antisite occupation decreases, the perpendicular magnetic anisotropy increases, and the Landau g factor exhibits a negative shift due to an increase in orbital momentum anisotropy. Our results will facilitate the design and exploration of new magnetic alloys with large magnetic anisotropy and desirable damping properties.

[1] T. Gerrits, H. A. M. van den Berg, J. Hohlfeld, L. Bar, and T. Rasing, Nature (London) **418**, 509 (2002).

[2] H. W. Schumacher, C. Chappert, R. C. Sousa, P. P. Freitas, and J. Miltat, Phys. Rev. Lett. **90**, 017204 (2003).

[3] S. I. Kiselev, J. C. Sankey, I. N. Krivorotov, N. C. Emley, R. J. Schoelkopf, R. A. Buhrman, and D. C. Ralph, Nature (London) **425**, 380 (2003).

[4] S. Kaka, M. R. Pufall, W. H. Rippard, T. J. Silva, S. E. Russek, and J. A. Katine, Nature (London) **437**, 389 (2005).

[5] A. Brataas, A. D. Kent, and H. Ohno, Nat. Mater. **11**, 372 (2012).

[6] P. Němec, E. Rozkotová, N. Tesařová, F. Trojánek, E. De Ranieri, K. Olejník, J. Zemen, V. Novák, M. Cukr, P. Malý, and T. Jungwirth, Nat. Phys. **8**, 411 (2012).

[7] L. Landau and E. Lifshitz, Phys. Z. Sowjetunion **8**, 153 (1935); T. L. Gilbert, Phys. Rev. **100**, 1243 (1955).

[8] T. L. Gilbert, IEEE Trans. Magn. **40**, 3443 (2004).

[9] J. C. Slonczewski, J. Magn. Magn. Mater. **159**, L1 (1996).

[10] B. Koopmans, J. J. M. Ruigrok, F. Dalla Longa, and W. J. M. de Jonge, Phys. Rev. Lett. **95**, 267207 (2005).

[11] A. D. Kent, Nat. Mater. **9**, 699 (2010).

[12] S. Ikeda, K. Miura, H. Yamamoto, K. Mizunuma, H. D. Gan, M. Endo, S. Kanai, J. Hayakawa, F. Matsukura, and H. Ohno, Nat. Mater. **9**, 721 (2010).

[13] W.-G. Wang, M. Li, S. Hageman, and C. L. Chien, Nat. Mater. **11**, 64 (2012).

[14] S. Mangin, D. Ravelosona, J. A. Katine, M. J. Carey, B. D. Terris, and E. E. Fullerton, Nat. Mater. **5**, 210 (2006).

[15] R. Urban, G. Woltersdorf, and B. Heinrich, Phys. Rev. Lett. **87**, 217204 (2001).

[16] D. J. Twisselmann and R. D. McMichael, J. Appl. Phys. **93**, 6903 (2003).

[17] G. Woltersdorf, M. Buess, B. Heinrich, and C. H. Back, Phys. Rev. Lett. **95**, 037401 (2005).

[18] A. Barman, S. Wang, J. Maas, A. R. Hawkins, S. Kwon, J. Bokor, A. Liddle, and H. Schmidt, Appl. Phys. Lett. **90**, 202504 (2007).

[19] A. Laraoui, J. Vénuat, V. Halté, M. Albrecht, E. Beaurepaire, and J.-Y. Bigot, J. Appl. Phys. **101**, 09C105 (2007).

[20] S. Mizukami, Y. Ando, and T. Miyazaki, Phys. Rev. B **66**, 104413 (2002).

[21] Y. Fan, X. Ma, F. Fang, J. Zhu, Q. Li, T. P. Ma, Y. Z. Wu, Z. H. Chen, H. B. Zhao, and G. Lupke, Phys. Rev. B **89**, 094428 (2014).

[22] V. Kamberský, Can. J. Phys. **48**, 2906 (1970); J. Kuneš and V. Kamberský, Phys. Rev. B **65**, 212411 (2002).

[23] B. Heinrich, D. Fraitová, and V. Kamberský, Phys. Status Solidi **23**, 501 (1967); V. Kamberský, Czech. J. Phys. B **26**, 1366 (1976); Phys. Rev. B **76**, 134416 (2007).

[24] D. Steiauf and M. Fähnle, Phys. Rev. B **72**, 064450 (2005).

[25] M. C. Hickey and J. S. Moodera, Phys. Rev. Lett. **102**, 137601 (2009).

[26] K. Gilmore, Y. U. Idzerda, and M. D. Stiles, Phys. Rev. Lett. **99**, 027204 (2007).

[27] K. Gilmore, Y. U. Idzerda, and M. D. Stiles, J. Appl. Phys. **103**, 07D303 (2008).

[28] A. Brataas, Y. Tserkovnyak, and G. E. W. Bauer, Phys. Rev. Lett. **101**, 037207 (2008).

[29] H. Ebert, S. Mankovsky, D. Ködderitzsch, and P. J. Kelly, Phys. Rev. Lett. **107**, 066603 (2011).

[30] Y. Liu, A. A. Starikov, Z. Yuan, and P. J. Kelly, Phys. Rev. B **84**, 014412 (2011).

[31] P. He, X. Ma, J. W. Zhang, H. B. Zhao, G. Lüpke, Z. Shi, and S. M. Zhou, Phys. Rev. Lett. **110**, 077203 (2013).

[32] J. Pelzl, R. Meckenstock, D. Spoddig, F. Schreiber, J. Pflaum, and Z. Frait, J. Phys. Condens. Matter **15**, S451 (2003).

[33] S. Ingvarsson, G. Xiao, S. Parkin, and R. Koch, Appl. Phys. Lett. **85**, 4995 (2004).

[34] F. Schreiber, J. Pflaum, Z. Frait, Th. Mühge, and J. Pelzl, Solid State Commun. **93**, 965 (1995).

[35] S. Mizukami, D. Watanabe, M. Oogane, Y. Ando, Y. Miura, M. Shirai, and T. Miyazaki, J. Appl. Phys. **105**, 07D306 (2009).

[36] M. Oogane, T. Kubota, Y. Kota, S. Mizukami, H. Naganuma, A. Sakuma, and Y. Ando, Appl. Phys. Lett. **96**, 252501 (2010).

[37] H. Lee, Y.-H. A. Wang, C. K. A. Mewes, W. H. Butler, T. Mewes, S. Maat, B. York, M. J. Carey, and J. R. Childress, Appl. Phys. Lett. **95**, 082502 (2009).

[38] S. Mizukami, E. P. Sajitha, D. Watanabe, F. Wu, T. Miyazaki, H. Naganuma, M. Oogane, and Y. Ando, Appl. Phys. Lett. **96**, 152502 (2010).

[39] S. Mizukami, S. Iihama, N. Inami, T. Hiratsuka, G. Kim, H. Naganuma, M. Oogane, and Y. Ando, Appl. Phys. Lett. **98**, 052501 (2011).

[40] S. Mizukami, F. Wu, A. Sakuma, J. Walowski, D. Watanabe, T. Kubota, X. Zhang, H. Naganuma, M. Oogane, Y. Ando, and T. Miyazaki, Phys. Rev. Lett. **106**, 117201 (2011).

[41] A. Barman, S. Wang, O. Hellwig, A. Berger, E. E. Fullerton, and H. Schmidt, J. Appl. Phys. **101**, 09D102 (2007).

[42] S. Pal, B. Rana, O. Hellwig, T. Thomson, and A. Barman, Appl. Phys. Lett. **98**, 082501 (2011).

[43] T. Qu and R. H. Victora, Effect of Substitutional Defects on Kambersky Damping in L10 Magnetic Materials (unpublished).

[44] J. O. Rantschler, R. D. McMichael, A. Castillo, A. J. Shapiro, W. F. Egelhoff Jr., B. B. Maranville, D. Pulugurtha, A. P. Chen, and L. M. Connors, J. Appl. Phys **101**, 033911 (2007).

[45] S. G. Reidy, L. Cheng, and W. E. Bailey, Appl. Phys. Lett. **82**, 1254 (2003).

[46] S. E. Russek, P. Kabos, R. D. McMichael, C. G. Lee, W. E. Bailey, R. Ewasko, and S. C. Sanders, J. Appl. Phys. **91**, 8659 (2002).

[47] S. Lihama, S. Mizukami, N. Inami, T. Hiratsuka, G. Kim, H. Naganuma, M. Oogane, T. Miyazaki, and Y. Ando, Japan. J. App. Phys. **52**, 073002 (2013).

[48] Smaller θ_H will lead to better suppression of extrinsic damping such as magnon-magnon scattering, but the magnetization precession signal probed with TRMOKE will be smaller, which induces the larger error bar in α_{eff}. The reason is that larger θ_H leads to the enhancement of magnetization precession in the polar direction, which creates a larger Kerr rotation signal compared with the longitudinal component. For all the TRMOKE measurements, the angle between magnetization and film normal, $\theta < 28°$, which results in a good suppression of the magnon-magnon scattering process.

[49] S. Okamoto, N. Kikuchi, O. Kitakami, T. Miyazaki, Y. Shimada, and K. Fukamichi, Phys. Rev. B **66**, 024413 (2002).

[50] J. Honolka, T. Y. Lee, K. Kuhnke, A. Enders, R. Skomski, S. Bornemann, S. Mankovsky, J. Minár, J. Staunton, H. Ebert, M. Hessler, K. Fauth, G. Schütz, A. Buchsbaum, M. Schmid, P. Varga, and K. Kern, Phys. Rev. Lett. **102**, 067207 (2009).

[51] J. P. Nibarger, R. Lopusnik, Z. Celinski, and T. J. Silva, App. Phys. Lett. **83**, 93 (2003).

[52] Small fluctuations of α_{eff} are observed at low fields. This might be due to the inaccuracy of the measurements since the number and amplitude of observed Kerr signal oscillations are small at low fields, which also increases the error bar in α_{eff} at lower fields.

[53] G. Malinowski, K. C. Kuiper, R. Lavrijsen, H. J. M. Swagten, and B. Koopmans, Appl. Phys. Lett. **94**, 102501 (2009).

[54] J. Lyubina, I. Opahle, M. Richter, O. Gutfleisch, K. Müller, and L. Schultz, App. Phys. Lett. **89**, 032506 (2006).

[55] J.-P. Kuang, M. Kontani, M. Matsui, and K. Adachi, Physica B **149**, 209 (1988).

[56] M. Chen, Z. Shi, W. J. Xu, X. X. Zhang, J. Du, and S. M. Zhou, App. Phys. Lett. **98**, 082503 (2011).

[57] The small deviation from the linear relationship at low x might be due to the fact that the weight of interband transitions through electron-phonon scattering is enhanced, which might contribute differently to α_0 compared with that of electron-impurity scattering.

[58] A. Alam, B. Kraczek, and D. D. Johnson, Phys. Rev. B **82**, 024435 (2010).

[59] C. J. Aas, L. Szunyogh, J. S. Chen, and R. W. Chantrell, App. Phys. Lett. **99**, 132501 (2011).

[60] P. Kamp, A. Marty, B. Gilles, R. Hoffmann, S. Marchesini, M. Belakhovsky, C. Boeglin, H. Durr, S. Dhesi, G. van der Laan, and A. Rogalev, Phys. Rev. B **59**, 1105 (1999).

[61] S. Dhesi, G. van der Laan, H. A. Durr, M. Belakhovsky, S. Marchesini, P. Kamp, A. Marty, B. Gilles, and A. Rogalev, J. Magn. Magn. Mat. **226–230**, 1580 (2001).

[62] X. Ma, P. He, L. Ma, G. Y. Guo, H. B. Zhao, S. M. Zhou, and G. Lüpke, Appl. Phys. Lett. **104**, 192402 (2014).